

1 Seasonal Prediction Skill of East Asian Summer Monsoon in CMIP5-Models

2 *Bo Huang,* Ulrich Cubasch, Christopher Kadow*

3 *Institute of Meteorology, Freie Universität Berlin,*
4 *Carl-Heinrich-Becker-Weg 6-10, 12165 Berlin, Germany*

5 *Email: huangb@live.com*

6

7 **ABSTRACT**

8 The East Asian summer monsoon (EASM) is an important part of the global climate system
9 and plays a vital role in the Asian climate. Its seasonal predictability is a long-standing issue
10 within the monsoon scientist community. In this study, we will analyse the seasonal (the
11 leading time is at least six months) prediction skill of the EASM rainfall and its associated
12 general circulation in non-initialised and initialised simulations for the years 1979-2005
13 which were performed by six prediction systems (*i.e.*, the BCC-CSM1-1, the CanCM4, the
14 GFDL-CM2p1, the HadCM3, the MIROC5 and the MPI-ESM-LR) from the Coupled Model
15 Intercomparison Project phase 5 (CMIP 5). We found that most prediction systems simulated
16 zonal wind over 850 and 200 hPa were significantly improved in the initialised simulations
17 compared to non-initialised simulations. Based on the knowledge that zonal wind indices can
18 be used as potential predictors for the EASM, we selected an EASM index based upon the
19 zonal wind over 850 hPa for further analysis. This assessment showed that the GFDL-CM2p1
20 and the MIROC5 added prediction skill in simulating the EASM index with initialisation, the
21 BCC-CSM1-1, the CanCM4, and the MPI-ESM-LR changed the skill insignificantly, and the
22 HadCM3 indicated a decreased skill score. The different response to the initialisation can be
23 traced back to the ability of the models to capture the ENSO (El Niño-Southern Oscillation)-
24 EASM coupled mode, particularly the Southern Oscillation-EASM coupled mode. As it is
25 known from observational studies, this mode links the oceanic circulation and the EASM
26 rainfall. On the whole, we find that the GFDL-CM2p1 and the MIROC5 are capable of
27 predicting the EASM on a seasonal time-scale under the current initialisation strategy.

28 **Key Words:** East Asian summer monsoon; initialisation; seasonal prediction; ENSO-EASM
29 coupled mode; CMIP5

30 **1. INTRODUCTION**

31 The Asian monsoon is the most powerful monsoon system in the world due to the thermal
32 contrast between the Eurasian continent and the Indo-Pacific Ocean. Its evolution and
33 variability critically influences the livelihood and the socio-economic status of over two
34 billion people who live in the Asian monsoon dominated region. It encompasses two sub-
35 monsoon systems, the South Asian monsoon (SAM) and the East Asian monsoon (EAM)
36 (Wang, 2006). In summer time (June-July-August), the EAM, namely, the East Asian
37 summer monsoon (EASM) occurs from the Indo-China peninsula to the Korean Peninsula
38 and Japan, and shows strong intraseasonal-to-interdecadal variability (Ding and Chan, 2005).
39 Thus, an accurate prediction of the EASM is an important and long-standing issue in climate
40 science.

41 To predict the EASM, there are two approaches, a statistical prediction and a dynamical
42 prediction, respectively. The statistical method seeks the relationship between the EASM and
43 a strong climate signal (e.g., ENSO, NAO; Wu et al., 2009;Yim et al., 2014;Wang et al.,
44 2015). This method establishes an empirical equation between the EASM and climate index.
45 However, it is limited by the strength of the climate signal. The other method is a dynamical
46 prediction. It employs a climate model to predict the EASM (Sperber et al., 2001;Kang and
47 Yoo, 2006;Wang et al., 2008a;Yang et al., 2008;Lee et al., 2010;Kim et al., 2012). Without
48 initialisation, both the atmosphere general circulation models (AGCMs) and the coupled
49 atmosphere-ocean general circulation models (CGCMs) cannot predict the climate on a
50 seasonal time-scale (Goddard et al., 2001). Given an initial condition, the AGCMs have the
51 ability to predict the climate, but show little skill in predicting the EASM (Wang et al.,
52 2005;Barnston et al., 2010). Because the AGCMs fail to produce a correct relationship
53 between the EASM and the sea surface temperature (SST) anomalies over the tropical
54 western North Pacific, the South China Sea, and the Bay of Bengal (Wang et al., 2004;Wang
55 et al., 2005), the monsoon community endeavours to predict the EASM with CGCMs (Wang
56 et al., 2008a;Zhou et al., 2009;Kim et al., 2012;Jiang et al., 2013).

57 CGCMs have proved to be the most valuable tools in predicting the EASM (Wang et
58 al., 2008a;Zhou et al., 2009;Kim et al., 2012;Jiang et al., 2013). However, the performance of
59 CGCMs in predicting the EASM on seasonal time-scale strongly depends on their ability to
60 reproduce the air-sea coupled process (Kug et al., 2008) and on the given initial condition
61 (Wang et al., 2005). In the coupled model inter-comparison project (CMIP) phase 3 (CMIP3;

Commented [BH1]: Minor comment

Commented [BH2]: Minor comment

Commented [BH3]: Minor comment

62 Meehl et al., 2007) era, the models simulate, not only a too weak tropical SST-monsoon
63 teleconnection (Kim et al., 2008; Kim et al., 2011), but also a too weak East Asian zonal
64 wind-rainfall teleconnection (Sperber et al., 2013). Compared to CMIP3 models, CMIP phase
65 5 (CMIP5; Taylor et al., 2012) models improved the representation of monsoon status
66 (Sperber et al., 2013). Therefore, given the initial conditions, the CMIP5 models do have the
67 potential to predict the EASM.

68 As mentioned, initial conditions do play a vital factor in predicting the EASM on sub-
69 seasonal to seasonal time-scale (Wang et al., 2005; Kang and Shukla, 2006). Under the
70 current set up of initialisation, the CMIP5 models showed the ability to predict the SST
71 variation index (*i.e.*, El Niño-Southern Oscillation-ENSO index; Niño3.4) of up to 15 months
72 in advance (Meehl and Teng, 2012; Meehl et al., 2014; Choi et al., 2016). This extended
73 prediction skill of the ENSO suggests that the EASM can be predicted on a seasonal time-
74 scale if the dynamical link between the ENSO and monsoon circulations is well represented
75 in these models. Two scientific questions will be addressed in this study: 1. How realistic are
76 the initialised CMIP5 models in representing the EASM? 2. Can the CMIP5 models capture
77 the dynamical link between the ENSO and EASM?

Commented [BH4]: Minor comment

78 In this paper, we will intercompare the influence of the initialisation on the capability of
79 the CMIP5 models to capture the EASM and the ENSO-EASM teleconnections. The model
80 simulations, comparison data and methods are introduced in Section 2. Section 3 describes
81 the seasonal skill of the rainfall predictions and the prediction of the associated general
82 circulation of the EASM. The mechanism causing the differential response of the models to
83 the initialisation is presented in Section 4. The discussions are shown in Section 5. Section 6
84 summarises the findings of this paper.

85 2. MODELS, DATA AND METHODS

86 2.1 MODELS AND INITIALISATION

87 In this study, we assessed six prediction systems from CMIP5 project (Table 1). The six
88 prediction systems have performed a yearly initialisation (Meehl et al., 2014). Their
89 simulations can be used in seasonal prediction study. There are two group of experiments,
90 without initialisation (non-initialisation) and with initialisation, respectively. For non-
91 initialised simulations, the models were forced by observed atmospheric composition changes
92 (reflecting both anthropogenic and natural sources) and, for the first time, including the time-
93 evolving land cover (Taylor et al., 2012). For initialised simulations, the models update the

94 time-evolving observed atmospheric and oceanic component (Taylor et al., 2012). Following
95 the CMIP5 framework, the six models established their initialisation strategy, which are
96 summarised in Table 2. More details about the initialisation strategy of each model can be
97 found in the reference paper in Table 1. To simplify the comparison, we select the first lead
98 year (up to 12 months) results for further analysis. The HadCM3-ff is the full-field initialised
99 simulation, which employs the same CGCM (HadCM3) as the anomaly initialisation. We
100 select the satellite era (1979 to 2005) for our study due to the spatial coverage of precipitation
101 observations.

102 The six models employ different initialisation strategies for atmospheric and oceanic
103 process, and for initial date (Table 2). These initialisation strategies contribute to a new
104 approach for climate prediction on decadal time-scale (Meehl et al., 2014). As the ocean is
105 driving the long-term prediction skill rather than the initial condition of the atmosphere, the
106 timing of the initialization has to be considered in the time scale of the ocean circulation, i.e.
107 years to decades. Therefore, on an ocean time scale, the initialization takes place with
108 comparable timing and therefore the results are comparable. This approach based on decadal
109 prediction experiments, which deviates from the scores of other seasonal prediction
110 experiments based on initialisation techniques derived from weather forecasting.

Commented [BH5]: Comment 1

111 2.2 COMPARISON DATA

112 The main datasets which were used for comparison in this study include: (1) monthly
113 precipitation data from the Global Precipitation Climatology Project (GPCP; Adler et al.,
114 2003); (2) monthly circulation data from ECMWF Interim re-analysis (ERA-Interim; Dee et
115 al., 2011); and (3) monthly mean SST from National Oceanic and Atmospheric
116 Administration (NOAA) improved Extended Reconstructed SST version 4 (ERSST v4;
117 Huang et al., 2015). All the model data and the comparison data are remapped onto a
118 common grid of 2.5°x2.5° by bi-linear interpolation to reduce the uncertainty induced by
119 different data resolutions.

120 2.3 EAST ASIAN MONSOON INDEX AND ENSO INDEX

121 In recent decades, more than 25 general circulation indices have been produced to
122 define the variability and the long-term change of the EASM. Wang et al. (2008b) arranged
123 them according to their ability to capture the main features of the EASM. They found that the
124 Wang and Fan index (hereafter WF-index; 1999) showed the best performance in capturing
125 the total variance of the precipitation and three-dimensional circulation over East Asia. We,

126 thus, select the WF-index for further analysis. Its definition is a standardised average zonal
 127 wind at 850 hPa in (5°-15°N, 90°-130°E) minus in (22.5°-32.5°N, 110°-140°E). The WF-
 128 index is a shear vorticity index which often is described by a north-south gradient of the zonal
 129 winds. In positive (negative) phase of the WF-index years, two strong (weak) rainfall belts
 130 located at the Indo China Peninsula-to-the Philippine Sea and the northern China-to-the
 131 Japanese Sea, and a weak (strong) rainfall belt occurs from the Yangtze river basin-to-the
 132 south of Japan. The June-July-August mean of WF-index is used to represent the EASM for
 133 further analysis in this study.

134 Here, we choose the Niño3.4 and southern oscillation index (SOI) to represents the
 135 ENSO status. The Niño3.4 is calculated by the SST anomaly in the central Pacific (190-
 136 240°E, 5°S-5°N), while the SOI is based upon the anomaly of the sea level pressure
 137 differences between Tahiti (210.75°E, 17.6°S) and Darwin (130.83°E, 12.5°S). To calculate
 138 the SOI, we interpolate the grid data to the Tahiti and the Darwin point by bilinear
 139 interpolation.

140 2.4 METHODS

141 In this study, we chose the un-centred Pattern Correlation Coefficient (PCC) (for more
 142 details see Barnett and Schlesinger, 1987) to analyse the model performance in comparison to
 143 the observational data, because centred correlations alone are not sufficient for the attribution
 144 of seasonal prediction (Mitchell et al., 2001). The un-centred PCC is defined by:

$$PCC = \frac{\sum_{x=1}^n \sum_{y=1}^m w_{(x,y)} F_{(x,y)} A_{(x,y)}}{\sqrt{\sum_{x=1}^n \sum_{y=1}^m w_{(x,y)} F_{(x,y)}^2 \sum_{x=1}^n \sum_{y=1}^m w_{(x,y)} A_{(x,y)}^2}}$$

145
 146 where n and m are grids on longitude and latitude, respectively. $F_{(x,y)}$ and $A_{(x,y)}$ represent two
 147 dimensions comparison and validating value. $w_{(x,y)}$ indicates the weighting coefficient for
 148 each grid. An equal weighting coefficient was applied in the study area.

149 We also employed the anomaly correlation coefficient (ACC) to analyse the model
 150 performance in reproducing observational variations. The ACC is the correlation between
 151 anomalies of forecasts and those of verifying values with the reference values, such as
 152 climatological values (Drosowsky and Zhang, 2003). Its definition is:

Commented [BH6]: Minor comment

$$ACC = \frac{\sum_{i=1}^n w_i (f_i - \bar{f})(a_i - \bar{a})}{\sqrt{\sum_{i=1}^n w_i (f_i - \bar{f})^2 \sum_{i=1}^n w_i (a_i - \bar{a})^2}}, (-1 \leq ACC \leq 1)$$

153

$$f_i = F_i - C_i, \bar{f} = \left(\sum_{i=1}^n w_i f_i \right) / \sum_{i=1}^n w_i$$

154

$$a_i = A_i - C_i, \bar{a} = \left(\sum_{i=1}^n w_i a_i \right) / \sum_{i=1}^n w_i$$

155

156 where n is the number of samples, and F_i , A_i , C_i represent comparison, verifying value,
 157 and reference value such as climatological value, respectively. Also, \bar{f} is the mean of f_i , \bar{a} is
 158 the mean of a_i , and w_i indicates the weighting coefficient. If the variation of anomalies of
 159 comparison dataset is a coincident with that of the anomalies of verifying value, ACC will
 160 take 1 (the maximum value). It indicates that the forecast has good skill.

Commented [BH7]: Minor comment

161 The root-mean-square-error (RMSE) is employed to check the model deviation from
 162 the observation and its definition is:

$$RMSE = \sqrt{\sum_{i=1}^n w_i D_i^2} / \sqrt{\sum_{i=1}^n w_i}$$

163

164 where D_i represents the deviation between comparison and verifying value, w_i is the
 165 weighting coefficient for each sample, and n is the number of samples. If RMSE is closer to
 166 zero, it means that the comparisons are closer to the verifying values.

167 3. SEASONAL PREDICTION SKILL OF THE EASM

168 The EASM has complex spatial and temporal structures that encompass the tropics,
 169 subtropics, and midlatitudes (Tao and Chen, 1987; Ding, 1994). In the late spring, an
 170 enhanced rainfall pattern was observed in the Indochina Peninsula and in the South China
 171 Sea. At the same time, the rainfall belt advances northwards to the south of China. In the
 172 early summer, the rainfall concentration occurred in the Yangtze River Basin and in southern
 173 Japan, namely, the Meiyu and Baiu seasons, respectively. The rainfall belt can reach as far as
 174 northern China, the Korean Peninsula (called the Changma rainy season) and central Japan in
 175 July (Ding, 2004; Ding and Chan, 2005).

176 The EASM is characterised by both seasonal heterogeneous rainfall distribution and
177 associated large-scale circulation systems (Wang et al., 2008b). In the summer season, water
178 moisture migrates from the Pacific Ocean to central and eastern Asia, which is carried by the
179 southwest surface winds. Generally, a strong summer monsoon year is followed by
180 precipitation in northern China, while a weak summer monsoon year is usually accompanied
181 by heavier rainfall along the Yangtze River basin (Ding, 1994; Zhou and Yu, 2005).

182 For multi-model ensemble mean (MME), the prediction skill of the June-July-August
183 mean rainfall and the associated general circulation variable (*i.e.*, zonal and meridional wind,
184 and mean sea level pressure) is presented in Figure 1. These variables have been widely used
185 to calculate the monsoon index (Wang et al., 2008b). Table 3 shows the contribution of these
186 variables in the EASM. Their abbreviations follow the guidelines of CMIP5 (Taylor et al.,
187 2012). Compared to the non-initialised experiment, a larger predicted area can be found in the
188 initialised experiment, especially for the psl, ua850 and ua200. There are small changes to the
189 predicted area between the non-initialised and initialised experiment for the pr, va850 and
190 va200. The individual model shows an acceptable performance (high PCC) in capturing the
191 observed spatial variation of the six variables, but a poor performance in simulating their
192 temporal variation (with low ACC) (Figure 2). There is no improvement in estimating the
193 spatial variation of the six variables with initialisation. We can see that the models show a
194 higher ACC in the initialised simulations than that in the non-initialised ones. The
195 improvement of simulating the temporal variation of zonal winds (*i.e.*, ua850 and ua200) is
196 larger than that of the rainfall and meridional winds. One can exploit this improvement by
197 using a general circulation based monsoon index as a tool to predict the EASM. As
198 mentioned in section 2.3, the WF-index better represents the monsoon rainfall and its
199 associated general circulation structure than the other monsoon index. Therefore, the
200 prediction skill of EASM in the following analysis is based on the WF-index.

201 In non-initialised simulations, none of the models captured the observed EASM, as
202 indicated by an insignificant ACC (Figure 3). The CanCM4 and the GFDL-CM2p1 simulate
203 a negative phase, while the BCC-CSM1-1, the HadCM3, the MIROC5 and the MPI-ESM-LR
204 all predicted a positive phase of the EASM. With initialisation, the GFDL-CM2p1 and the
205 MIROC5 improved the skill to simulate the EASM, the CanCM4 and the MPI-ESM-LR
206 displayed hardly any reaction, while the BCC-CSM1-1 and the HadCM3 showed a worse
207 performance than without initialisation. Particularly with anomaly initialisation, the HadCM3

208 significantly lost its prediction skill in capturing the EASM. The CMIP5 models showed
209 different response to the initialisation in predicting the EASM on seasonal time-scale. To
210 understand the potential reason, we analysed the principle components of six variables, which
211 contributed to the EASM. The details are presented in Section 4.

212 4. EASM-ENSO COUPLED MODE IN CMIP5

213 We employed the EOF method to analyse the leading EOF modes of the six meteorological
214 variables anomaly in the EASM region (0° - 50° N, 100° - 140° E). The first EOF mode of the
215 rainfall is characterised by a “sandwich” pattern, which showed sharp contrast between the
216 prominent rainfall centre over Malaysia, the Yangtze River valley and the south of Japan, and
217 the enhanced rainfall over the Indo-China Peninsula and the Philippine Sea (Figure 4). The
218 increased precipitation is associated with cyclones in the low-level (850 hPa) and anti-
219 cyclones in the upper level (200 hPa).

220 The correlation coefficient of the first eigenvector and the associated principal
221 component (PC) between the model simulation and the observation in the non-initialised and
222 the initialised simulation is presented in Figure 5. The models captured the eigenvector of the
223 first EOF for the six meteorological fields in non-initialised simulation. However, they failed
224 to reproduce the associated PC of the first leading EOF mode. Compared to the non-
225 initialised simulation, the models showed no improvement to simulate the first leading EOF
226 mode of rainfall, but exhibit a better performance in representing the first leading EOF mode
227 of zonal wind. The CanCM4 and the GFDL-CM2p1 captured the first PC of ua850, but not
228 the other five models. For the zonal wind at 200 hPa, the BCC-CSM1-1 fails to simulate its
229 first EOF mode while the other six models can. Only the GFDL-CM2p1 accurately simulates
230 the first EOF eigenvectors and the associated PC of va850, which cannot be reproduced in the
231 other models. No models captured the spatial-temporal variation of the first EOF mode of
232 meridional wind at 200 hPa. In addition, the GFDL-CM2p1 and the MIROC5 simulates a
233 reasonable leading EOF mode and associated PC of psl, while the other models do not
234 capture it.

235 Figure 6 shows the fractional (percentage) variances of the six variables from the first
236 EOF mode with the total variances from the observation, and the model simulation with
237 (with-out) initialisation. The observational total variances for the pr, the ua850, the ua200, the
238 va850, the va200 and the psl, are depicted by the first lead EOF mode in 21.2, 59.0, 36.5,
239 20.6, 28.5 and 50.0 percent, respectively. The models simulated the comparable explanatory

240 variances, which showed a slight discrepancy for the first leading mode in the non-
241 initialisation. From non-initialised simulation to initialised simulation, the CGCMs tended to
242 enhance the first EOF leading mode because they show larger fractional variances of the total
243 variances of the six variables. We note that the CanCM4 and the GFDL-CM2p1 significantly
244 increased the fractional variances from non-initialisation to initialisation.

245 The ENSO is a dominant mode of the inter-annual variability of the coupled ocean and
246 atmosphere climate system, which has strong effects on the inter-annual variation of the
247 EASM (Wang et al., 2000; Wu et al., 2003). Wang et al. (2015) summarised that the first EOF
248 lead mode of the ASM is ENSO developing mode. As previously mentioned, the first EOF
249 mode was improved in the initialised simulations, compared to the non-initialised simulation.
250 This also can be found in the ENSO indices (Figure 7). The individual members and their
251 ensemble mean of the six models show a low correlation coefficient to the observational
252 Niño3.4 and the SOI in the non-initialised simulations. These two indices showed strong anti-
253 phases in the observation, with the correlation range being -0.94 to -0.92 for four seasons
254 (DJF, MAM, JJA, SON). Without initialisation, the models can describe the anti-correlation
255 between Niño3.4 and the SOI, but with weaker correlation. Compared to the non-
256 initialisation, there is a significant improvement for models in capturing the observational
257 Niño3.4 and the SOI in the initialised experiments. The initialisation lowers the spread of
258 Niño3.4 and the SOI in all the six models. There is a noticeable change between the model in
259 producing the relationship between the Niño3.4 and the SOI. We found that the GFDL-
260 CM2p1 (HadCM3) shows a lower (higher) Niño3.4-SOI correlation in initialisation than that
261 in non-initialisation. With initialisation, the ensemble mean of each model outperforms its
262 individual members in capturing Niño3.4 and the SOI, while without initialisation it showed
263 a worse performance than that of the individual members in simulating Niño3.4 and the SOI.

264 The EASM strongly relies on the pre-seasons ENSO signal due to the lag response of
265 the atmosphere to the SST anomaly (Wu et al., 2003). The lead-lag correlation coefficients
266 between the EASM index and the Niño3.4, and the SOI from JJA(-1) to JJA(+1) are
267 illustrated in Figure 8. The pre-season Niño3.4 (SOI) presents a significant negative
268 (positive) correlation to the EASM, while the post-season Niño3.4 (SOI) showed a notable
269 positive (negative) correlation. This lead-lag correlation coefficient phase is called the
270 Niño3.4-/SOI-EASM coupled mode (Wang et al., 2008b). In the non-initialised cases, the
271 models do not produce the teleconnection between the ENSO and the EASM. The CanCM4,

272 the HadCM3 and the MPI-ESM-LR failed to represent the lead-lag correlation coefficient
273 differences between pre-/post-season ENSO and EASM. The BCC-CSM1-1, the GFDL-
274 CM2p1 and the MIROC5 captured the coupled mode of the ENSO and the EASM. However,
275 the pre-season ENSO has a weak effect on the EASM. Compared to the non-initialised cases,
276 the MIROC5 and the GFDL-CM2p1 both demonstrated a significant improvement in
277 simulating Niño3.4 (SOI)-EASM coupled mode in the initialisation. The BCC-CSM1-1, the
278 HadCM3, and the HadCM3-ff showed no improvement, with insignificant correlation
279 between Niño3.4 (SOI) and the EASM. The CanCM4 and the MPI-ESM-LR indicated a
280 higher correlation between the EASM and the simultaneous-to-post-season ENSO than to the
281 pre-season ENSO.

282 5. DISCUSSION

283 The model exhibits a better performance in simulating the general circulation of the
284 EASM with initialisation. Thus, initialisation is helpful in forecasting the EASM on a
285 seasonal time-scale. There are two initialisation methods in our study, full-field initialisation
286 and anomaly initialisation (Table 1). The full-field initialisation produces more skilful
287 predictions on the seasonal time-scale in predicting regional temperature and precipitation
288 (Magnusson et al., 2013;Smith et al., 2013). Nevertheless, for predicting the EASM, there is
289 no significant difference between the two methods. We can see that both the GFDL-CM2p1
290 and the MIROC5 have a significant improvement in capturing the EASM, with full-field and
291 anomaly initialisation, respectively. Only the HadCM3 was initialised by the two
292 initialisation techniques. However, both these two initialised techniques are producing poor
293 predictions of the EASM with no major differences.

294 The current initialisation strategy updates the observed atmospheric component (*i.e.*,
295 zonal and meridional wind, geopotential height, *etc.*) and the SST (Meehl et al., 2009;Taylor
296 et al., 2012;Meehl et al., 2014). With initialisation, the SST conveys its information via the
297 large heat content of the ocean to the coupled system. Therefore, an index indicating an ocean
298 oscillation like Niño3.4 showed a seasonal-to-decadal prediction skill (Jin et al., 2008;Luo et
299 al., 2008;Choi et al., 2016). The models studied here demonstrated a prediction skill in
300 simulating Niño3.4 and the SOI due to this effect. The change of the correlation between
301 Niño3.4 and the SOI is insignificant from non-initialised to initialised simulations. We
302 therefore conclude that the relationship between Niño3.4 and the SOI depends more on the
303 model parameterisation than on the initial condition.

304 Wang *et al.* (2015) found that the second EOF mode of ASM is the Indo-western
305 Pacific monsoon-ocean coupled mode, the third is the Indian Ocean dipole (IOD) mode, and
306 the fourth is the trend mode. The Indo-western Pacific monsoon-ocean coupled mode is the
307 atmosphere-ocean interaction mode (Wang *et al.*, 2013;Xiang *et al.*, 2013), which is
308 supported by a positive thermodynamic feedback between the western North Pacific (WNP)
309 anticyclone and the underlying Indo-Pacific sea surface temperature anomaly dipole over the
310 warm pool (Wang *et al.*, 2015). The IOD increases the precipitation from the South Asian
311 subcontinent to southeastern China and suppresses the precipitation over the WNP (Wang *et*
312 *al.*, 2015). It affects the Asian monsoon by the meridional asymmetry of the monsoonal
313 easterly shear during the boreal summer, which can particularly strengthen the northern
314 branch of the Rossby wave response to the south-eastern Indian Ocean SST cooling, leading
315 to an intensified monsoon flow as well as an intensified convection (Wang and Xie,
316 1996;Wang *et al.*, 2003;Xiang *et al.*, 2011;Wang *et al.*, 2015). We noted that the models
317 simulate a reasonable first EOF mode, but illustrate no skill in capturing the other EOF
318 leading modes (not shown). We argue that the models cannot well represent the monsoon-
319 ocean interaction, even with initialisation. The models do not simulate the third EOF leading
320 mode of the EASM since the predictability of the IOD extends only over a three-month time-
321 scale (Choudhury *et al.*, 2015). The current initialisation strategies (both anomaly and full
322 field) enhance the ENSO signal in the model simulations with higher explained fraction of
323 variance. Kim *et al.* (2012) described a similar finding in ECMWF System 4 and NCEP
324 Climate Forecast System version 2 (CFSv2) seasonal prediction simulations. With
325 initialisation, the models well predict ENSO on seasonal time-scale, which leads to an overly
326 strong modulation of the EASM by ENSO (Jin *et al.*, 2008;Kim *et al.*, 2012).

327 It is worth mentioning that it was an extremely weak monsoon and strong El Niño year
328 in 1998. The CanCM4, the GFDL-CM2p1, the MIROC5 and the MPI-ESM-LR have the
329 ability to simulate the extreme monsoon event, while the BCC-CSM1-1, and the HadCM3 do
330 not capture it even with initialisation. There is the potential for the BCC-CSM and the
331 HadCM models to improve the teleconnection between the ENSO and the EASM.

332 This study has discussed six CMIP5 models in predicting the EASM on seasonal time-
333 scale. The six models are earth system coupled models which present a better SST-monsoon
334 teleconnection than CMIP3 models (Sperber *et al.*, 2013) and IRI (International Research
335 Institute for Climate and Society) models (Barnston *et al.*, 2010). There are 4 AGCMs

336 contributing to the IRI prediction system, including ECHAM4.5, CCM3.6, COLA and
337 GFDL-AM2p14. These models are forced to forecast the climate on seasonal time-scale by
338 prescribed SST. Barnston et al. (2010) found that the models showed low prediction skill
339 over East Asia. Therefore, the IRI prediction system cannot be used to predict the EASM.
340 There are two seasonal forecast application systems, the ECMWF System and the NCEP
341 CFS, respectively. Both the two application systems have low prediction skill of EASM (Kim
342 et al., 2012;Jiang et al., 2013). The CMIP5 models have potential to be developed as
343 application system for EASM seasonal prediction, especially the GFDL-CM2p1 and the
344 MIROC5.

345 **To better predict the short-to-long term climate, World Climate Research Programme**
346 **(WCRP) launched two new projects, i.e., Climate-system Historical Forecast Project (CHFP;**
347 **Kirtman and Pirani, 2009;Tompkins et al., 2017) and Subseasonal-to-Seasonal (S2S)**
348 **Prediction Project (Vitart et al., 2017). The two projects coordinate most climate modelling**
349 **research group and provide a large range of forecast dataset. A comprehensive comparison of**
350 **all the CHFP and S2S data with the CMIP5 simulations regard to the seasonal prediction skill**
351 **of the EASM is certainly an interesting topic, which should be addressed in an additional**
352 **paper.**

Commented [BH8]: Comment 2

353 We have compared six CMIP5 systems with their respective initialisation strategies.
354 The GFDL-CM2p1 and the MIROC5 have the potential to serve as seasonal forecast
355 application system even with their current initialisation method. These models have great
356 potential to optimise the SST-EASM interaction simulation performance to improve their
357 seasonal prediction skill of the EASM.

358 6. SUMMARY

359 Six earth system models from CMIP5 have been selected in this study. We have analysed the
360 improvement of the rainfall, the mean sea level pressure, the zonal wind and the meridional
361 wind in the EASM region from non-initialisation to initialisation. The low prediction skill of
362 the summer monsoon precipitation is due to the uncertainties of cloud physics and cumulus
363 parameterisations in the models (Lee et al., 2010;Seo et al., 2015). The models showed a
364 better performance in capturing the inter-annual variability of zonal wind than the
365 precipitation after initialisation. Thus, the zonal wind index is an additional factor, which can
366 indicate the prediction skill of the model. When, we calculate the WF-index in both non-
367 initialised and initialised simulations, the GFDL-CM2p1 and the MIROC5 showed a

368 significant advancement in simulating the EASM from non-initialised to initialised
369 simulation with a lower RMSE and a higher ACC. There is only a slight change in the WF-
370 index calculated from the BCC-CSM1-1, the CanCM4 and the MPI-ESM-LR data with
371 initialisation. Compared to the non-initialised simulation, the HadCM3 loses prediction skill,
372 especially with anomaly initialisation.

373 To test the possible mechanisms of the models' performance in the non-initialisation
374 and the initialisation, we have calculated the leading mode of the six fields, which are
375 associated to the EASM. The models demonstrated a better agreement with the observational
376 first EOF mode in the initialised simulations. The first lead mode of zonal wind at 200 hPa
377 showed a significant improvement in the models except the BCC-CSM1-1 with initialisation.
378 Therefore, a potential predictor might be an index based upon the zonal wind at 200 hPa.
379 Compared to the non-initialisation, the models enhanced the first EOF mode with a higher
380 fraction of variance to the total variance after initialisation. The first EOF mode of the EASM
381 is the ENSO developing mode (Wang et al., 2015). We have analysed the seasonal simulating
382 skill of Niño3.4 and the SOI in each model. The models showed a poor performance in
383 representing Niño3.4 and the SOI in the non-initialised simulation. Initialisation improved the
384 model simulating skill of Niño3.4 and the SOI. The initialised simulations decreased the
385 spread of ensemble members in the models. We found that there is no significant change in
386 the models reproducing the correlation between Niño3.4 and the SOI from non-initialisation
387 to initialisation.

388 In general, the pre-season warm phase of the ENSO (El Niño) leads to a weak EASM
389 producing more rainfall over the South China Sea and northwest China, and less rainfall over
390 the Yangtze River Valley and the southern Japan; the cold phase of the ENSO (La Niña)
391 illustrated a reverse rainfall pattern to El Niño in East Asia. The pre-season Niño3.4 (SOI)
392 exhibits a strong negative (positive) correlation to the EASM, while the correlation between
393 the post-season Niño3.4 (SOI) and the EASM illustrated an anti-phase as the pre-season. In
394 the non-initialised simulations, the models do not capture Niño3.4-/SOI-EASM coupled
395 mode. We found that only the MIROC5 has the ability to represent the Niño3.4-EASM
396 coupled mode with initialisation. For the SOI-EASM coupled mode, the GFDL-CM2p1 and
397 the MIROC5 captured it in the initialisation, while the BCC-CSM1-1, the HadCM3, the
398 HadCM2-ff, the CanCM4 and the MPI-ESM-LR do not. Therefore, we argue that the

399 differential depiction of ENSO-EASM coupled mode in CMIP5 models lead to their
400 differential response to initialisation.

401 **Acknowledgements**

402 The China Scholarship Council (CSC) and the Freie Universität Berlin supported this work.
403 We would like to thank the climate modelling groups listed in Table 1 of this paper for
404 producing and making their model output available. We acknowledge the MiKlip project
405 funded by the Federal Ministry of Education and Research and the German Climate
406 Computing Centre (DKRZ) for providing the data services. We are grateful to Mrs
407 Margerison Patricia for her useful comments and the proofreading work on this manuscript.

408 **References**

409 Adler, R. F., Huffman, G. J., Chang, A., Ferraro, R., Xie, P.-P., Janowiak, J., Rudolf, B.,
410 Schneider, U., Curtis, S., Bolvin, D., Gruber, A., Susskind, J., Arkin, P., and Nelkin, E.: The
411 Version-2 Global Precipitation Climatology Project (GPCP) Monthly Precipitation Analysis
412 (1979–Present), *J Hydrometeorol*, 4, 1147-1167, 10.1175/1525-
413 7541(2003)004<1147:tvGPCP>2.0.CO;2, 2003.
414 Arora, V. K., Scinocca, J. F., Boer, G. J., Christian, J. R., Denman, K. L., Flato, G. M.,
415 Kharin, V. V., Lee, W. G., and Merryfield, W. J.: Carbon emission limits required to satisfy
416 future representative concentration pathways of greenhouse gases, *Geophys Res Lett*, 38,
417 L05805, 10.1029/2010gl046270, 2011.
418 Barnett, T. P., and Schlesinger, M. E.: Detecting Changes in Global Climate Induced by
419 Greenhouse Gases, *J Geophys Res Atmos*, 92, 14772-14780, 10.1029/JD092iD12p14772,
420 1987.
421 Barnston, A. G., Li, S. H., Mason, S. J., DeWitt, D. G., Goddard, L., and Gong, X. F.:
422 Verification of the First 11 Years of IRI's Seasonal Climate Forecasts, *J Appl Meteorol Clim*,
423 49, 493-520, 10.1175/2009jamc2325.1, 2010.
424 Choi, J., Son, S. W., Ham, Y. G., Lee, J. Y., and Kim, H. M.: Seasonal-to-Interannual
425 Prediction Skills of Near-Surface Air Temperature in the CMIP5 Decadal Hindcast
426 Experiments, *J Clim*, 29, 1511-1527, 10.1175/Jcli-D-15-0182.1, 2016.
427 Choudhury, D., Sharma, A., Sivakumar, B., Sen Gupta, A., and Mehrotra, R.: On the
428 predictability of SSTA indices from CMIP5 decadal experiments, *Environ Res Lett*, 10,
429 074013, 10.1088/1748-9326/10/7/074013, 2015.
430 Dee, D. P., Uppala, S. M., Simmons, A. J., Berrisford, P., Poli, P., Kobayashi, S., Andrae, U.,
431 Balmaseda, M. A., Balsamo, G., Bauer, P., Bechtold, P., Beljaars, A. C. M., van de Berg, L.,
432 Bidlot, J., Bormann, N., Delsol, C., Dragani, R., Fuentes, M., Geer, A. J., Haimberger, L.,
433 Healy, S. B., Hersbach, H., Holm, E. V., Isaksen, I., Kallberg, P., Kohler, M., Matricardi, M.,
434 McNally, A. P., Monge-Sanz, B. M., Morcrette, J. J., Park, B. K., Peubey, C., de Rosnay, P.,
435 Tavolato, C., Thepaut, J. N., and Vitart, F.: The ERA-Interim reanalysis: configuration and
436 performance of the data assimilation system, *Q J R Meteorol Soc*, 137, 553-597,
437 10.1002/qj.828, 2011.
438 Delworth, T. L., Broccoli, A. J., Rosati, A., Stouffer, R. J., Balaji, V., Beesley, J. A., Cooke,
439 W. F., Dixon, K. W., Dunne, J., Dunne, K. A., Durachta, J. W., Findell, K. L., Ginoux, P.,
440 Gnanadesikan, A., Gordon, C. T., Griffies, S. M., Gudgel, R., Harrison, M. J., Held, I. M.,
441 Hemler, R. S., Horowitz, L. W., Klein, S. A., Knutson, T. R., Kushner, P. J., Langenhorst, A.

442 R., Lee, H. C., Lin, S. J., Lu, J., Malyshev, S. L., Milly, P. C. D., Ramaswamy, V., Russell, J.,
 443 Schwarzkopf, M. D., Shevliakova, E., Sirutis, J. J., Spelman, M. J., Stern, W. F., Winton, M.,
 444 Wittenberg, A. T., Wyman, B., Zeng, F., and Zhang, R.: GFDL's CM2 global coupled climate
 445 models. Part I: Formulation and simulation characteristics, *J Clim*, 19, 643-674,
 446 10.1175/Jcli3629.1, 2006.
 447 Ding, Y.: Seasonal march of the East-Asian summer monsoon., in: *East Asian Monsoon*,
 448 edited by: Chang, C.-P., World Scientific, Singapore, 560, 2004.
 449 Ding, Y. H.: *Monsoons over China*, Kluwer Academic Publisher, Dordrecht/Boston/London,
 450 419 pp., 1994.
 451 Ding, Y. H., and Chan, J. C. L.: The East Asian summer monsoon: an overview, *Meteorol*
 452 *Atmos Phys*, 89, 117-142, 10.1007/s00703-005-0125-z, 2005.
 453 Drosowsky, W., and Zhang, H.: Verification of Spatial Fields, in: *Forecast Verification: A*
 454 *Practitioner's Guide in Atmospheric Science* edited by: Jolliffe, L. T., and Stephenson, D. B.,
 455 John Wiley & Sons Ltd, England, 128-129, 2003.
 456 Goddard, L., Mason, S. J., Zebiak, S. E., Ropelewski, C. F., Basher, R., and Cane, M. A.:
 457 Current approaches to seasonal-to-interannual climate predictions, *Int J Climatol*, 21, 1111-
 458 1152, 10.1002/joc.636, 2001.
 459 Huang, B. Y., Banzon, V. F., Freeman, E., Lawrimore, J., Liu, W., Peterson, T. C., Smith, T.
 460 M., Thorne, P. W., Woodruff, S. D., and Zhang, H. M.: Extended Reconstructed Sea Surface
 461 Temperature Version 4 (ERSST.v4). Part I: Upgrades and Intercomparisons, *J Clim*, 28, 911-
 462 930, 10.1175/Jcli-D-14-00006.1, 2015.
 463 Jiang, X. W., Yang, S., Li, Y. Q., Kumar, A., Liu, X. W., Zuo, Z. Y., and Jha, B.: Seasonal-
 464 to-Interannual Prediction of the Asian Summer Monsoon in the NCEP Climate Forecast
 465 System Version 2, *J Clim*, 26, 3708-3727, 10.1175/Jcli-D-12-00437.1, 2013.
 466 Jin, E. K., Kinter, J. L., Wang, B., Park, C. K., Kang, I. S., Kirtman, B. P., Kug, J. S., Kumar,
 467 A., Luo, J. J., Schemm, J., Shukla, J., and Yamagata, T.: Current status of ENSO prediction
 468 skill in coupled ocean-atmosphere models, *Clim Dyn*, 31, 647-664, 10.1007/s00382-008-
 469 0397-3, 2008.
 470 Kang, I.-S., and Shukla, J.: Dynamic seasonal prediction and predictability of the monsoon,
 471 in: *The Asian Monsoon*, edited by: Wang, B., Springer Berlin Heidelberg, Berlin, Heidelberg,
 472 585-612, 2006.
 473 Kang, I. S., and Yoo, J. H.: Examination of multi-model ensemble seasonal prediction
 474 methods using a simple climate system, *Clim Dyn*, 26, 285-294, 10.1007/s00382-005-0074-8,
 475 2006.
 476 Kim, H. J., Wang, B., and Ding, Q. H.: The Global Monsoon Variability Simulated by
 477 CMIP3 Coupled Climate Models, *J Clim*, 21, 5271-5294, 10.1175/2008jcli2041.1, 2008.
 478 Kim, H. J., Takata, K., Wang, B., Watanabe, M., Kimoto, M., Yokohata, T., and Yasunari, T.:
 479 Global Monsoon, El Nino, and Their Interannual Linkage Simulated by MIROC5 and the
 480 CMIP3 CGCMs, *J Clim*, 24, 5604-5618, 10.1175/2011jcli4132.1, 2011.
 481 Kim, H. M., Webster, P. J., Curry, J. A., and Toma, V. E.: Asian summer monsoon prediction
 482 in ECMWF System 4 and NCEP CFSv2 retrospective seasonal forecasts, *Clim Dyn*, 39,
 483 2975-2991, 10.1007/s00382-012-1470-5, 2012.
 484 Kirtman, B., and Pirani, A.: The State of the Art of Seasonal Prediction Outcomes and
 485 Recommendations from the First World Climate Research Program Workshop on Seasonal
 486 Prediction, *Bull Am Meteorol Soc*, 90, 455-458, 10.1175/2008bams2707.1, 2009.
 487 Kug, J. S., Kang, I. S., and Choi, D. H.: Seasonal climate predictability with Tier-one and
 488 Tier-two prediction systems, *Clim Dyn*, 31, 403-416, DOI 10.1007/s00382-007-0264-7, 2008.
 489 Lee, J.-Y., Wang, B., Kang, I. S., Shukla, J., Kumar, A., Kug, J. S., Schemm, J. K. E., Luo, J.
 490 J., Yamagata, T., Fu, X., Alves, O., Stern, B., Rosati, T., and Park, C. K.: How are seasonal

491 prediction skills related to models' performance on mean state and annual cycle?, *Clim Dyn*,
492 35, 267-283, 10.1007/s00382-010-0857-4, 2010.

493 Luo, J.-J., Masson, S., Behera, S. K., and Yamagata, T.: Extended ENSO Predictions Using a
494 Fully Coupled Ocean–Atmosphere Model, *J Clim*, 21, 84-93, 10.1175/2007jcli1412.1, 2008.

495 Magnusson, L., Alonso-Balmaseda, M., Corti, S., Molteni, F., and Stockdale, T.: Evaluation
496 of forecast strategies for seasonal and decadal forecasts in presence of systematic model
497 errors, *Clim Dyn*, 41, 2393-2409, 10.1007/s00382-012-1599-2, 2013.

498 Matei, D., Pohlmann, H., Jungclaus, J., Muller, W., Haak, H., and Marotzke, J.: Two Tales of
499 Initializing Decadal Climate Prediction Experiments with the ECHAM5/MPI-OM Model, *J*
500 *Clim*, 25, 8502-8523, 10.1175/Jcli-D-11-00633.1, 2012.

501 Meehl, G., Covey, C., Delworth, T., Latif, M., McAvaney, B., Mitchell, J., Stouffer, R., and
502 Taylor, K.: The WCRP CMIP3 multi-model dataset: a new era in climate change research,
503 *Bull Am Meteorol Soc*, 88, 1383-1394, 2007.

504 Meehl, G. A., Goddard, L., Murphy, J., Stouffer, R. J., Boer, G., Danabasoglu, G., Dixon, K.,
505 Giorgetta, M. A., Greene, A. M., Hawkins, E., Hegerl, G., Karoly, D., Keenlyside, N.,
506 Kimoto, M., Kirtman, B., Navarra, A., Pulwarty, R., Smith, D., Stammer, D., and Stockdale,
507 T.: DECADAL PREDICTION Can It Be Skillful?, *Bull Am Meteorol Soc*, 90, 1467-1485,
508 10.1175/2009bams2778.1, 2009.

509 Meehl, G. A., and Teng, H. Y.: Case studies for initialized decadal hindcasts and predictions
510 for the Pacific region, *Geophys Res Lett*, 39, L22705, 10.1029/2012gl053423, 2012.

511 Meehl, G. A., Goddard, L., Boer, G., Burgman, R., Branstator, G., Cassou, C., Corti, S.,
512 Danabasoglu, G., Doblas-Reyes, F., Hawkins, E., Karspeck, A., Kimoto, M., Kumar, A.,
513 Matei, D., Mignot, J., Msadek, R., Navarra, A., Pohlmann, H., Rienecker, M., Rosati, T.,
514 Schneider, E., Smith, D., Sutton, R., Teng, H. Y., van Oldenborgh, G. J., Vecchi, G., and
515 Yeager, S.: DECADAL CLIMATE PREDICTION An Update from the Trenches, *Bull Am*
516 *Meteorol Soc*, 95, 243-267, 10.1175/Bams-D-12-00241.1, 2014.

517 Mitchell, J. F. B., Karoly, D. J., Hegerl, G. C., Zwiers, F. W., Allen, M. R., and Marengo, J.:
518 Detection of Climate Change and Attribution of Causes, in: *Third Assessment Report of the*
519 *Intergovernmental Panel on Climate Change.*, edited by: Houghton, J. T., Griggs, D. J.,
520 Noguer, M., van der Linden, P. J., Dai, X., Maskell, K., and Johnson, C. A., Cambridge
521 University Press, New York, 470, 2001.

522 Seo, K. H., Son, J. H., Lee, J. Y., and Park, H. S.: Northern East Asian Monsoon Precipitation
523 Revealed by Airmass Variability and Its Prediction, *J Clim*, 28, 6221-6233, 10.1175/Jcli-D-
524 14-00526.1, 2015.

525 Smith, D. M., Eade, R., and Pohlmann, H.: A comparison of full-field and anomaly
526 initialization for seasonal to decadal climate prediction, *Clim Dyn*, 41, 3325-3338,
527 10.1007/s00382-013-1683-2, 2013.

528 Sperber, K., Annamalai, H., Kang, I. S., Kitoh, A., Moise, A., Turner, A., Wang, B., and
529 Zhou, T.: The Asian summer monsoon: an intercomparison of CMIP5 vs. CMIP3 simulations
530 of the late 20th century, *Clim Dyn*, 41, 2711-2744, 10.1007/s00382-012-1607-6, 2013.

531 Sperber, K. R., Brankovic, C., Deque, M., Frederiksen, C. S., Graham, R., Kitoh, A.,
532 Kobayashi, C., Palmer, T., Puri, K., Tennant, W., and Volodin, E.: Dynamical seasonal
533 predictability of the Asian summer monsoon, *Mon Weather Rev*, 129, 2226-2248,
534 10.1175/1520-0493(2001)129<2226:Dspota>2.0.Co;2, 2001.

535 Tao, S. Y., and Chen, L. X.: A review of recent research on the East Asian summer monsoon
536 in China, in: *Monsoon Meteorology*, edited by: Chang, C.-P., and Krishnamurti, T. N., Oxford
537 University Press, Oxford, 60-92, 1987.

538 Tatebe, H., Ishii, M., Mochizuki, T., Chikamoto, Y., Sakamoto, T. T., Komuro, Y., Mori, M.,
539 Yasunaka, S., Watanabe, M., Ogochi, K., Suzuki, T., Nishimura, T., and Kimoto, M.: The

540 Initialization of the MIROC Climate Models with Hydrographic Data Assimilation for
 541 Decadal Prediction, *J Meteorol Soc Japan*, 90a, 275-294, 10.2151/jmsj.2012-A14, 2012.
 542 Taylor, K. E., Stouffer, R. J., and Meehl, G. A.: An Overview of CMIP5 and the Experiment
 543 Design, *Bull Am Meteorol Soc*, 93, 485-498, 10.1175/Bams-D-11-00094.1, 2012.
 544 Tompkins, A. M., Ortiz De Zarate, M. I., Saurral, R. I., Vera, C., Saulo, C., Merryfield, W. J.,
 545 Sigmond, M., Lee, W. S., Baehr, J., Braun, A., Butler, A., Deque, M., Doblas-Reyes, F. J.,
 546 Gordon, M., Scaife, A. A., Imada, Y., Ishii, M., Ose, T., Kirtman, B., Kumar, A., Muller, W.
 547 A., Pirani, A., Stockdale, T., Rixen, M., and Yasuda, T.: The Climate-System Historical
 548 Forecast Project: Providing Open Access to Seasonal Forecast Ensembles from Centers
 549 around the Globe, *Bull Am Meteorol Soc*, 98, 2293-2302, 10.1175/Bams-D-16-0209.1, 2017.
 550 Vitart, F., Ardilouze, C., Bonet, A., Brookshaw, A., Chen, M., Codorean, C., Deque, M.,
 551 Ferranti, L., Fucile, E., Fuentes, M., Hendon, H., Hodgson, J., Kang, H. S., Kumar, A., Lin,
 552 H., Liu, G., Liu, X., Malguzzi, P., Mallas, I., Manoussakis, M., Mastrangelo, D., MacLachlan,
 553 C., McLean, P., Minami, A., Mladek, R., Nakazawa, T., Najm, S., Nie, Y., Rixen, M.,
 554 Robertson, A. W., Ruti, P., Sun, C., Takaya, Y., Tolstykh, M., Venuti, F., Waliser, D.,
 555 Woolnough, S., Wu, T., Won, D. J., Xiao, H., Zaripov, R., and Zhang, L.: The Subseasonal to
 556 Seasonal (S2s) Prediction Project Database, *Bull Am Meteorol Soc*, 98, 163-+,
 557 10.1175/Bams-D-16-0017.1, 2017.
 558 Wang, B., and Xie, X.: Low-Frequency Equatorial Waves in Vertically Sheared Zonal Flow.
 559 Part I: Stable Waves, *J Atmos Sci*, 53, 449-467, 10.1175/1520-
 560 0469(1996)053<0449:lfewiv>2.0.co;2, 1996.
 561 Wang, B., and Fan, Z.: Choice of south Asian summer monsoon indices, *Bull Am Meteorol*
 562 *Soc*, 80, 629-638, 10.1175/1520-0477(1999)080<0629:Cosasm>2.0.Co;2, 1999.
 563 Wang, B., Wu, R. G., and Fu, X. H.: Pacific-East Asian teleconnection: how does ENSO
 564 affect East Asian climate?, *J Clim*, 13, 1517-1536, 2000.
 565 Wang, B., Wu, R., and Li, T.: Atmosphere–Warm Ocean Interaction and Its Impacts on
 566 Asian–Australian Monsoon Variation*, *J Clim*, 16, 1195-1211, 10.1175/1520-
 567 0442(2003)16<1195:aoiaii>2.0.co;2, 2003.
 568 Wang, B., Kang, I.-S., and Lee, J.-Y.: Ensemble Simulations of Asian–Australian Monsoon
 569 Variability by 11 AGCMs*, *J Clim*, 17, 803-818, 10.1175/1520-
 570 0442(2004)017<0803:esoamv>2.0.co;2, 2004.
 571 Wang, B., Ding, Q. H., Fu, X. H., Kang, I. S., Jin, K., Shukla, J., and Doblas-Reyes, F.:
 572 Fundamental challenge in simulation and prediction of summer monsoon rainfall, *Geophys*
 573 *Res Lett*, 32, L15711, 10.1029/2005gl022734, 2005.
 574 Wang, B.: *The Asian Monsoon*, Springer Science & Business Media, Praxis, New York, NY,
 575 USA, 2006.
 576 Wang, B., Lee, J.-Y., Kang, I.-S., Shukla, J., Park, C. K., Kumar, A., Schemm, J., Cocke, S.,
 577 Kug, J. S., Luo, J. J., Zhou, T., Wang, B., Fu, X., Yun, W. T., Alves, O., Jin, E. K., Kinter, J.,
 578 Kirtman, B., Krishnamurti, T., Lau, N. C., Lau, W., Liu, P., Pegion, P., Rosati, T., Schubert,
 579 S., Stern, W., Suarez, M., and Yamagata, T.: Advance and prospectus of seasonal prediction:
 580 assessment of the APCC/ClipAS 14-model ensemble retrospective seasonal prediction
 581 (1980–2004), *Clim Dyn*, 33, 93-117, 10.1007/s00382-008-0460-0, 2008a.
 582 Wang, B., Wu, Z. W., Li, J. P., Liu, J., Chang, C. P., Ding, Y. H., and Wu, G. X.: How to
 583 measure the strength of the East Asian summer monsoon, *J Clim*, 21, 4449-4463,
 584 10.1175/2008jcli2183.1, 2008b.
 585 Wang, B., Xiang, B., and Lee, J. Y.: Subtropical high predictability establishes a promising
 586 way for monsoon and tropical storm predictions, *Proc Natl Acad Sci U S A*, 110, 2718-2722,
 587 10.1073/pnas.1214626110, 2013.

588 Wang, B., Lee, J. Y., and Xiang, B. Q.: Asian summer monsoon rainfall predictability: a
589 predictable mode analysis, *Clim Dyn*, 44, 61-74, 10.1007/s00382-014-2218-1, 2015.
590 Wu, R. G., Hu, Z. Z., and Kirtman, B. P.: Evolution of ENSO-related rainfall anomalies in
591 East Asia, *J Clim*, 16, 3742-3758, 10.1175/1520-0442(2003)016<3742:Eoerai>2.0.Co;2,
592 2003.
593 Wu, T. W., Song, L. C., Li, W. P., Wang, Z. Z., Zhang, H., Xin, X. G., Zhang, Y. W., Zhang,
594 L., Li, J. L., Wu, F. H., Liu, Y. M., Zhang, F., Shi, X. L., Chu, M., Zhang, J., Fang, Y. J.,
595 Wang, F., Lu, Y. X., Liu, X. W., Wei, M., Liu, Q. X., Zhou, W. Y., Dong, M., Zhao, Q. G., Ji,
596 J. J., Li, L., and Zhou, M. Y.: An Overview of BCC Climate System Model Development and
597 Application for Climate Change Studies, *J Meteorol Res-Prc*, 28, 34-56, 10.1007/s13351-
598 014-3041-7, 2014.
599 Wu, Z. W., Wang, B., Li, J. P., and Jin, F. F.: An empirical seasonal prediction model of the
600 east Asian summer monsoon using ENSO and NAO, *J Geophys Res Atmos*, 114, D18120,
601 10.1029/2009jd011733, 2009.
602 Xiang, B., Wang, B., Yu, W., and Xu, S.: How can anomalous western North Pacific
603 Subtropical High intensify in late summer?, *Geophys Res Lett*, 40, 2349-2354,
604 10.1002/grl.50431, 2013.
605 Xiang, B. Q., Yu, W. D., Li, T., and Wang, B.: The critical role of the boreal summer mean
606 state in the development of the IOD, *Geophys Res Lett*, 38, L02710, 10.1029/2010gl045851,
607 2011.
608 Yang, S., Zhang, Z. Q., Kousky, V. E., Higgins, R. W., Yoo, S. H., Liang, J. Y., and Fan, Y.:
609 Simulations and seasonal prediction of the Asian summer monsoon in the NCEP Climate
610 Forecast System, *J Clim*, 21, 3755-3775, 10.1175/2008jcli1961.1, 2008.
611 Yim, S. Y., Wang, B., and Xing, W.: Prediction of early summer rainfall over South China by
612 a physical-empirical model, *Clim Dyn*, 43, 1883-1891, 10.1007/s00382-013-2014-3, 2014.
613 Zhou, T., Wu, B., and Wang, B.: How Well Do Atmospheric General Circulation Models
614 Capture the Leading Modes of the Interannual Variability of the Asian–Australian Monsoon?,
615 *J Clim*, 22, 1159-1173, 10.1175/2008jcli2245.1, 2009.
616 Zhou, T. J., and Yu, R. C.: Atmospheric water vapor transport associated with typical
617 anomalous summer rainfall patterns in China, *J Geophys Res Atmos*, 110, D08104,
618 10.1029/2004jd005413, 2005.
619

Table 1. Details of the prediction systems investigated in this study.

System	Institute	Resolution		Non- Initialisation		Initialisation Type	Reference
		Atmospheric	Oceanic	Members	Members		
BCC-CSM1-1	Beijing Climate Center, China	T42L26	11onx1.33lat L40	3	3	Full-field	Wu <i>et al.</i> (2014)
CanCM4	Canadian Centre for Climate Modelling and Analysis, Canada	T63L35	256 x 192 L40	10	10	Full-field	Arora <i>et al.</i> (2011)
GFDL-CM2p1	Geophysical Fluid Dynamics Laboratory, USA	N45L24	11on x 0.33-1lat L50	10	10	Full-field	Delworth <i>et al.</i> (2006)
HadCM3	Met Office Hadley Centre, UK	N48L19	1.25x1.25 L20	10	10 + 10	Full-field and Anomaly	Smith <i>et al.</i> (2013)
MIROC5	Atmosphere and Ocean Research Institute, Japan	T85L40	256x192 L44	5	6	Anomaly	Tatebe <i>et al.</i> (2012)
MPI-ESM-LR	Max Planck Institute for Meteorology, Germany	T63L47	GR15 L40	3	3	Anomaly	Matei <i>et al.</i> (2012)

622 Table 2. Brief summaries of initialisation strategies used by modelling groups in the study. ECMWF: European Centre for Medium-Range
 623 Weather Forecasts; GODAS: Global Ocean Data Assimilation System; NCEP: National Centers for Environmental Prediction; S: Salinity;
 624 SODA: Simple Ocean Data Assimilation; T: Temperature.

system	Atmosphere	Ocean	Initialised date	Internet
BCC-CSM1-1	-	integration with ocean T nudged to SODA product above 1500 m	Ensemble 1: 1 st September Ensemble 2: 1 st November Ensemble 3: 1 st January	http://forecast.bccsm.ncc-cma.net/
CanCM4	ECMWF re-analysis	off-line assimilation of SODA and GODAS subsurface ocean T and S adjusted to reserve model T-S	1 st January	http://www.ccma.ec.gc.ca/
GFDL-CM2p1	GFDL re-analysis	assimilates observations of T, S from World Ocean Database	1 st November	https://www.gfdl.noaa.gov/multidecadal-prediction-stream/
HadCM3	ECMWF re-analysis	off-line ocean re-analysis product	1 st January	http://cerawww.dkrz.de/WDCC/CMIP5/
MIROC5	-	integration using observational gridded ocean T and S	1 st January	http://amaterasu.ees.hokudai.ac.jp/
MPI-ESM-LR	NCEP re-analysis	off-line ocean hindcast forced with NCEP	1 st January	http://cerawww.dkrz.de/WDCC/CMIP5/

625

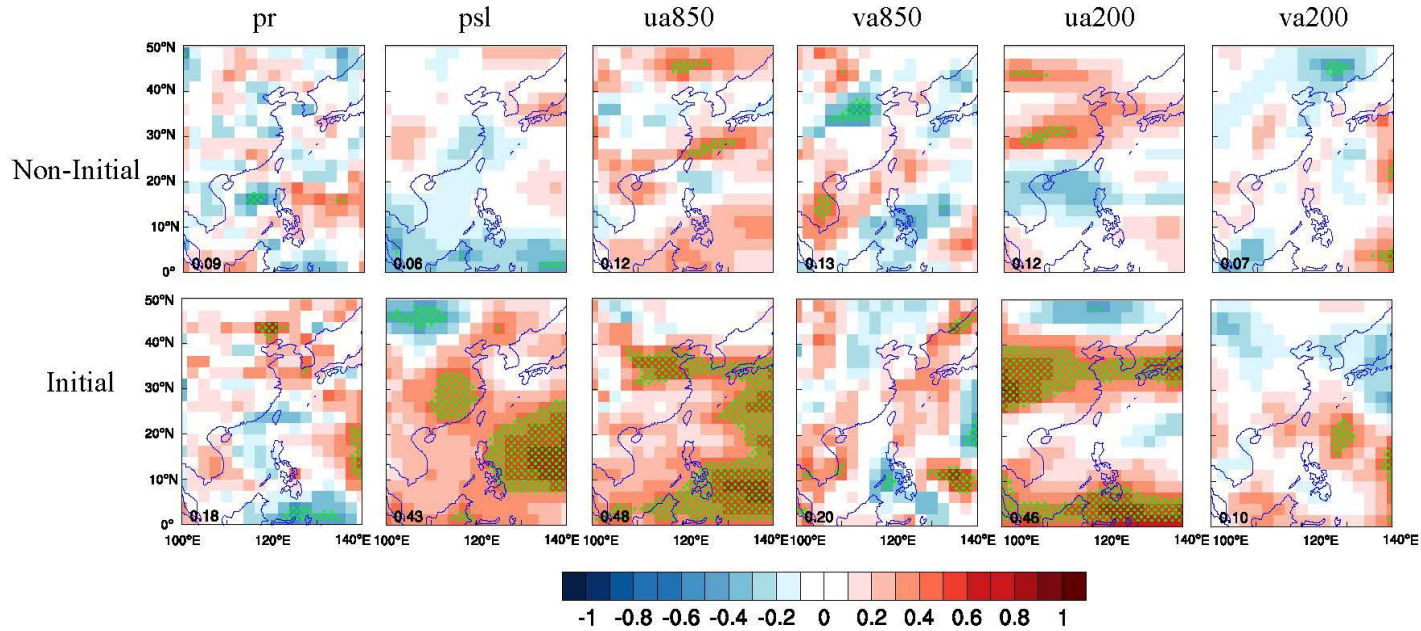
626 Table 3. Description of the six variables which contribute to the EASM. The abbreviation of these variables is followed to the guidelines of
 627 CMIP5.

variable	Standard name	Contribution to the EASM
pr	Precipitation	Precipitation distribution indicates the strength of EASM
psl	Mean sea surface pressure	Differences of mean sea surface pressure between land and ocean lead to EASM
ua850	Zonal winds over 850 hPa	A component of low-level cyclone which transports vapor from ocean to land
va850	Meridional winds over 850 hPa	As ua850, and contributes to Hadley's cell
va200	Meridional winds over 850 hPa	A component of upper-level Hadley's cell
ua200	Zonal winds over 850 hPa	As va200

628

629

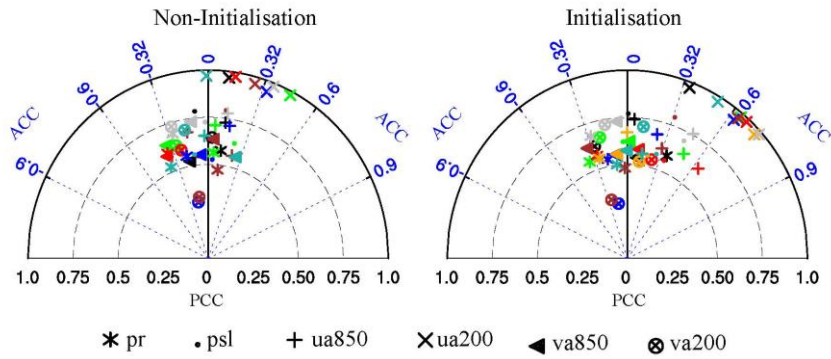
630



631

632 Fig. 1. Anomaly correlation coefficient of six variables (i.e. precipitation, mean sea level pressure, and winds over 850 hPa and 200 hPa)
 633 between multi-model ensemble mean and observations in non-initialisation and initialisation. The green dotted grids illustrate the significant
 634 level at 0.05. The number at lower left corner indicates the ratio of significant grid points to entire grids. The GPCP was employed as the
 635 reference data for precipitation (pr) while winds (i.e. ua850, va850, ua200 and va200) and mean sea level pressure (psl) were compared with
 636 ERA-Interim re-analysis.

637

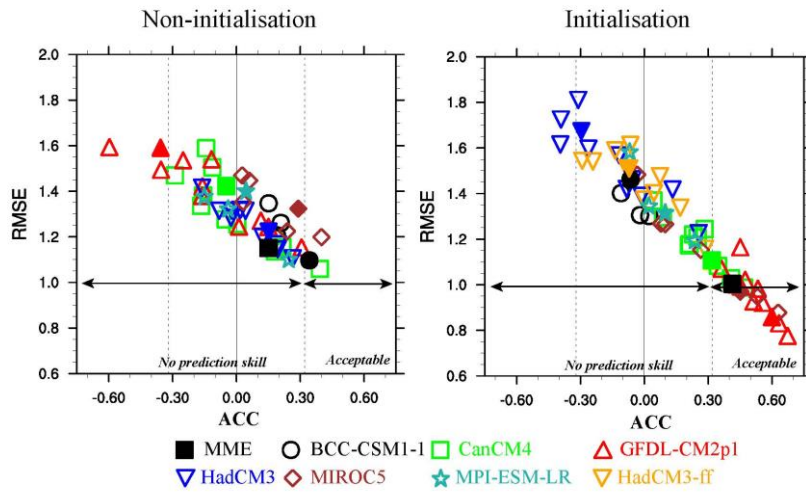


638

639 Fig.2. Taylor diagrams display of pattern (PCC) and temporal (ACC) correlation
640 metrics of six variables between observation and model simulation in the EASM
641 region (0-50°N, 100-140°E). Each coloured marker represents a model, *i.e.*, the BCC-
642 CSM1-1 (black), the CanCM4 (green), the GFDL-CM2p1 (red), the HadCM3 (blue),
643 the MIROC5 (brown), the MPI-ESM-LR (light-sea-blue), and the HadCM3-ff
644 (orange).

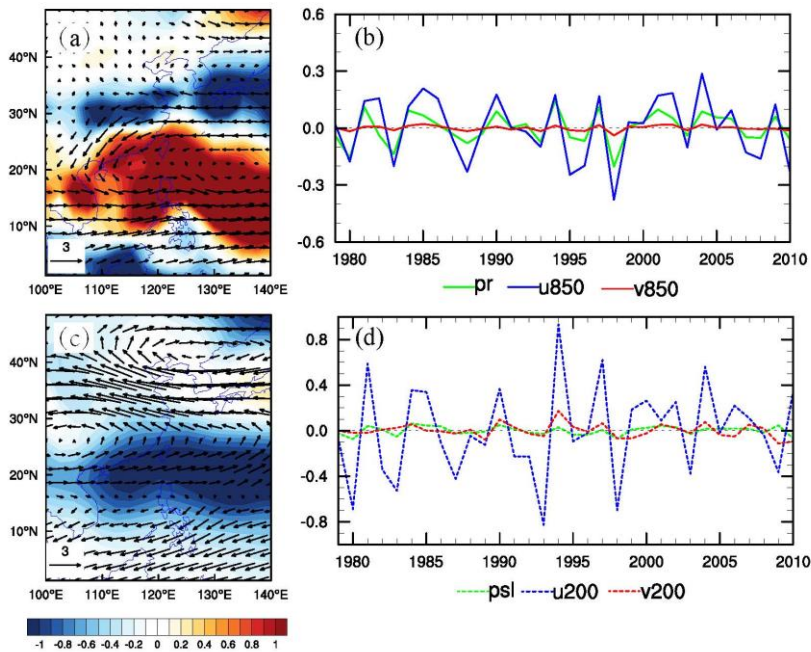
645

646



647

648 Fig. 3. Performance of the model ensemble member (hollow marker) and its ensemble
649 mean (solid marker) on the EASM index. The abscissa and ordinates are the anomaly
650 correlation coefficient (ACC) and the root-mean-square-error (RMSE), respectively.
651 The observed EASM index is calculated by zonal wind at 850 hPa from the ERA-
652 Interim re-analysis data. The black dot lines indicate the significant level at 0.1. The
653 vertical black line represents the correlation between the simulating and the
654 observational EASM index is 0.



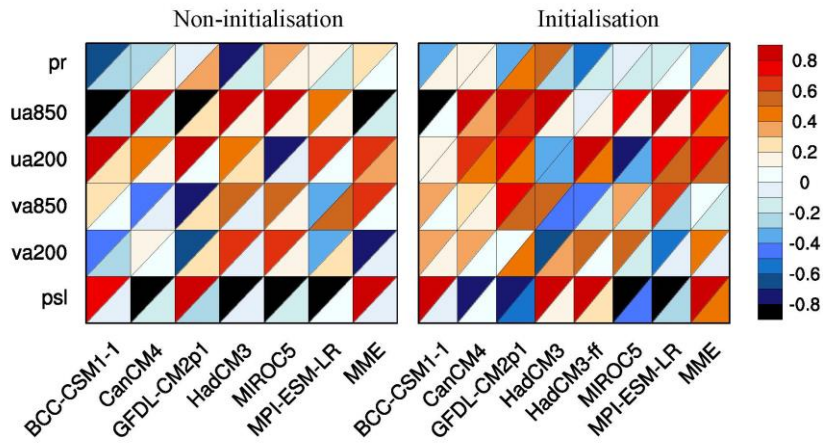
655

656 Fig. 4. Spatial distribution of observational of the first leading EOF mode of June-
 657 July-August precipitation and winds over 850 hPa (a), mean sea level pressure and
 658 winds over 200 hPa (c) and the associated principal component (PC; b, d). The GPCP
 659 and ERA-Interim data from 1979-2005 were used for the EOF analysis in the EASM
 660 domain.

661

662

663

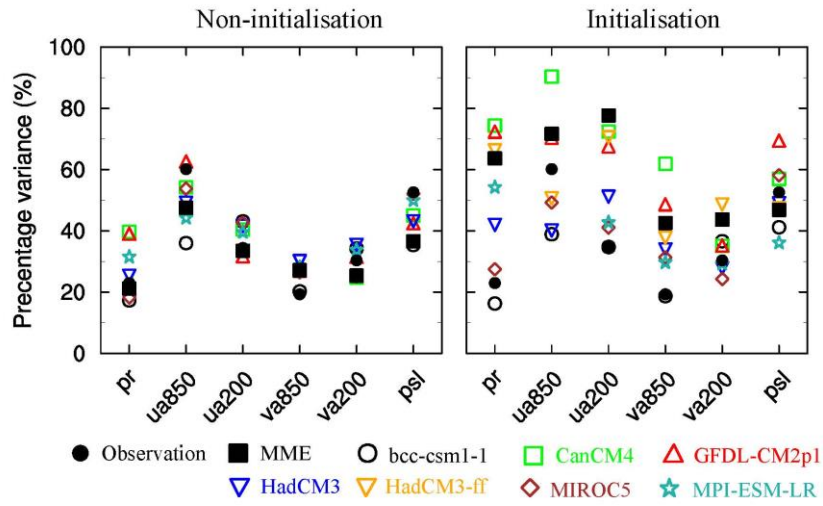


664

665 Fig. 5. Portrait diagram display of correlation metrics between the observation and the
666 model simulation of the first lead EOF mode for the six fields in the non-initialisation
667 (left) and the initialisation (right). Each grid square is split by a diagonal in order to
668 show the correlation with respect to both the eigenvector (upper left triangle) and its
669 associated principal components (lower right triangle) reference data sets.

670

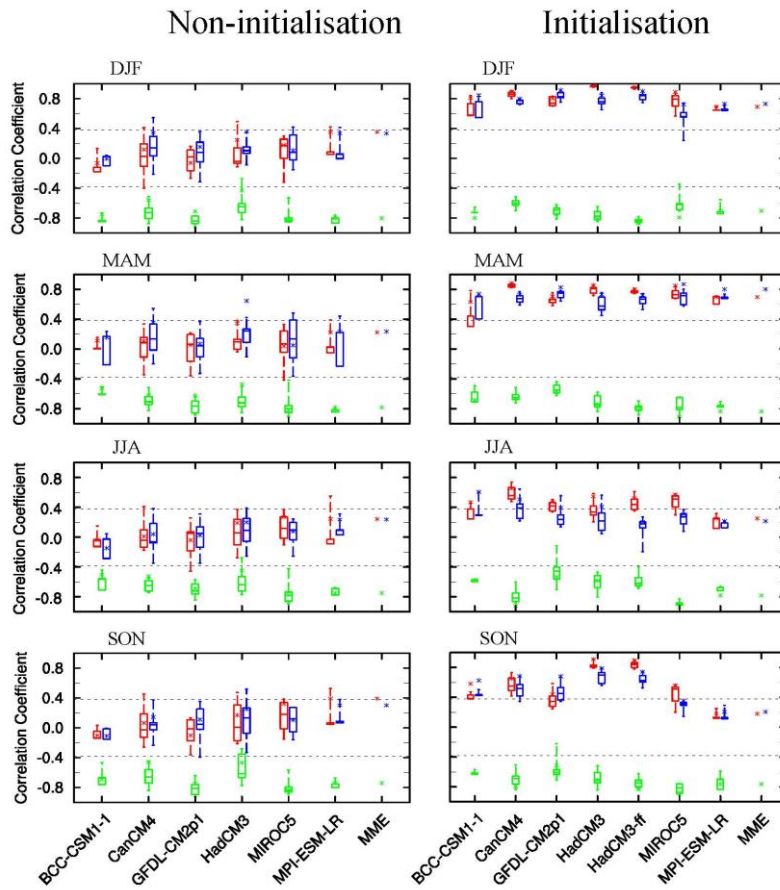
671



672

673 Fig. 6. Fraction variance (%) explained by the first EOF mode for six fields in the
674 non-initialisation (left) and the initialisation (right).

675



676

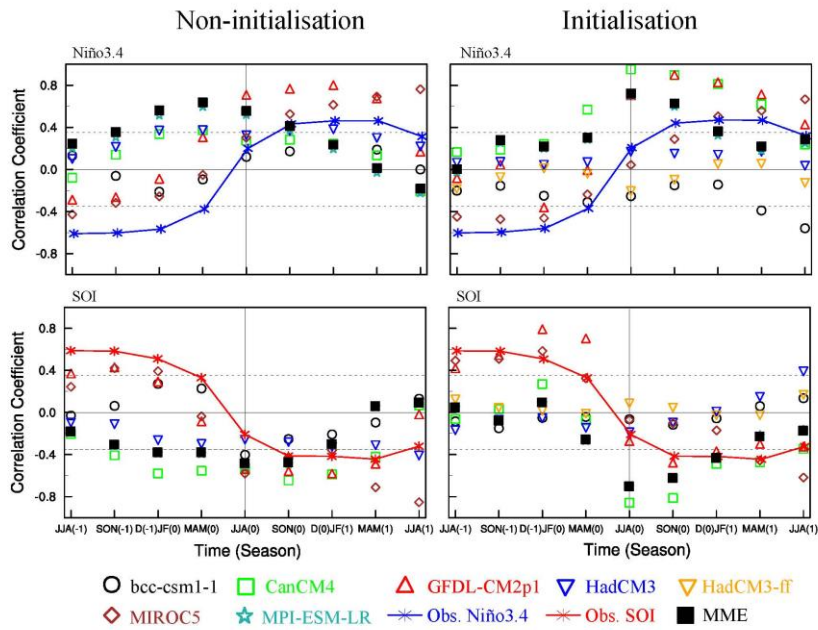
677 Fig. 7. Model prediction skill in representing the observational Niño3.4 (red), the SOI
 678 (blue) from the DJF to SON in non-initialisation (left) and initialisation (right). Green
 679 diagram shows the correlation coefficient between the model simulated Niño3.4 and
 680 the SOI. Box and whisker diagram shows ensemble mean of each model (asterisk),
 681 median (horizontal line), 25th and 75th percentiles (box), minimum and maximum
 682 (whisker). The two black dotted lines indicate 0.05 significant level based upon
 683 Student's t-test.

684

685

686

687



688

689 Fig. 8. Lead-lag correlation coefficients between the EASM index and Niño3.4
690 (upper), and SOI (lower) in non-initialised simulations (left) and initialised ones
691 (right) for observation (marker line) and models (marker) from JJA(-1) to JJA(+1).
692 The two black dotted lines are 0.05 significant level based upon Student's t-test. The
693 vertical line represents JJA(0), where the simultaneous correlations between the
694 EASM index and Niño3.4, and SOI are shown.

695